ACS Sustainable Resource Management

pubs.acs.org/acssrm

Article

Life Cycle Assessment of Silver, Copper, and Zinc-Based Metal−Organic Framework Products for Industry-Scale Production and Future Horizons

Mostafa Dadashi Firouzjaei,*# Mohsen Pilevar,# Rilyn Todd, Delanie Williams, Mahshid Mardani, Farhad Akbari Afkhami, Mohtada Sadrzadeh, Mona Bavarian, and Mark Elliott*

Cite This: *ACS Sustain. Resour. Manag.* 2026, 3, 717−732

Read Online

ACCESS | Metrics & More | Article Recommendations | Supporting Information

ABSTRACT: Metal−organic frameworks (MOFs) are an increasingly versatile nanomaterial platform, whose functional properties make them highly attractive for diverse industrial applications. In this work, we perform a dosage-normalized cradle-to-gate life cycle assessment of three benchmark MOFs (silver-, copper-, and zinc-based) against the commercial antibiotic levofloxacin under both lab-scale and projected industrial-scale scenarios. We find that, while silver-MOF achieves the lowest functional mass per application, its environmental footprint is dominated by the precursor synthesis, whereas copper- and zinc-MOFs deliver more balanced impact profiles when normalized to performance. Process-grouping analysis pinpoints metal precursor production and solvent use as critical hotspots, informing targeted strategies—such as closed-loop metal recovery, green solvent substitution, and continuous-flow intensification—for sustainable scale-up. By embedding experimentally determined minimum bactericidal concentrations (MBCs) into TRACI 2.1 metrics, our study establishes a transferable, performance-based framework for benchmarking emerging nanomaterials against traditional antimicrobial agents and highlights clear levers to accelerate the sustainable industrial deployment of MOF technologies.

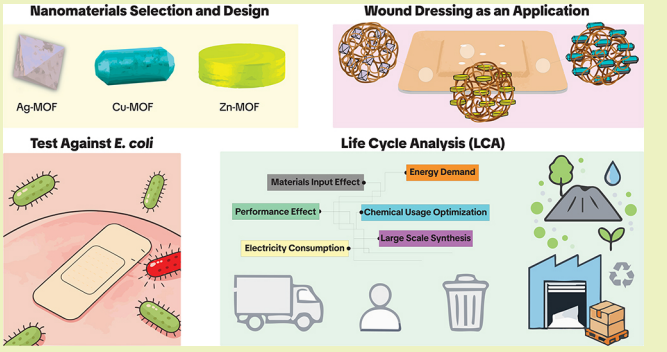

KEYWORDS: *metal−organic frameworks (MOFs), life cycle assessment (LCA), antimicrobial resistance, eco-efficiency, process intensification, waste valorization*

1. INTRODUCTION

Metal−organic frameworks (MOFs) have emerged as one of the most exciting classes of materials in recent decades, distinguished by their exceptionally high surface areas, tunable porosity, and versatile chemistry.[1] Due to their unique physicochemical properties, MOFs have been extensively investigated for a wide range of applications, including gas storage, carbon capture, catalysis, and chemical separation.[2] MOFs have also been explored in emerging areas, such as antimicrobial coatings and water treatment, where the controlled release of metal ions and/or the encapsulation of bioactive agents imparts antibacterial activity.[3−9] This breadth of functionality underscores their potential across energy, environmental remediation, and health technologies.[10] However, despite their vast potential, most MOFs remain far from realization at an industrial scale, with only a few examples being produced beyond the laboratory scale (Table S1).[11] This gap between bench-scale innovation and commercial deployment highlights the need to address questions of scalable manufacturing and sustainability early in the development of MOFs.

A major challenge in translating MOF research to industry lies in the complexity of mass production.[12] Syntheses that are straightforward at the gram scale often become impractical or cost-prohibitive at kilogram or tonne scales.[13] Conventional solvothermal routes rely on high-boiling organic solvents, such as *N*,*N*-dimethylformamide (DMF), and require long reaction times, generating hazardous waste and increasing energy demand.[12,14] In particular, the pervasive use of DMF raises serious sustainability concerns, as scaling conventional recipes would produce substantial volumes of toxic solvent waste with attendant environmental and health risks.[15] Accordingly, rigorous quantification of waste and solvent intensity and the pursuit of solvent-lean, recoverable, or aqueous pathways are critical for viable high-volume manufacturing.

Received: September 24, 2025
Revised: January 21, 2026
Accepted: January 23, 2026
Published: February 27, 2026

Moreover, scaling up is not simply a matter of enlarging the reactor, it requires re-engineering with explicit attention to raw material sustainability, process efficiency, product quality, and downstream processing.[16] Recent efforts by both academic and industrial groups have started to emphasize greener synthesis routes in response to these challenges.[17−20] In particular, the principles of green chemistry are increasingly seen as essential guidelines for MOF production, driven in part by tightening environmental regulations and the imperative of sustainable development in the chemical industry.[21,22] In this context, life cycle assessment (LCA) emerges as a vital tool for guiding the sustainable industrialization of MOFs.

LCA provides a holistic assessment of the environmental impacts associated with a material or process, from raw material extraction and synthesis ("cradle") to product use and end-of-life disposal ("grave").[23] Applying LCA to MOF development reveals the often-overlooked aspects of scale-up, including energy consumption, resource usage, emissions, and waste generation, across each step of MOF production. Early studies have demonstrated the importance of such an approach. For example, an LCA of the zeolitic imidazolate framework (ZIF-8) found that even laboratory-scale production carries substantial burdens, dominated by solvent use and energy inputs.[24] This finding implies that if MOFs are to be deployed for sustainability-driven applications (such as carbon capture or low-energy separations), then their fabrication processes must be critically evaluated and improved; otherwise, the upstream impacts could undermine the downstream benefits.[24] More broadly, key sustainability metrics—raw material consumption, energy demand, and overall environmental impact—should be integrated into MOF research from the outset. Many MOFs contain metal nodes and organic linkers that require significant resources to produce, and their synthesis can be energy-intensive.[25] Without strategies to recycle solvents, reclaim unreacted precursors, or utilize renewable energy, the carbon footprint and waste output of MOF production can be substantial.[26] LCA offers a quantitative framework to pinpoint such "hotspots" in the production chain and to compare alternative synthesis routes on a consistent environmental basis.

To the best of our knowledge, this study represents the first systematic life cycle assessment comparing a series of MOFs synthesized and experimentally evaluated within the same laboratory framework, using antibacterial performance metrics derived under consistent assay conditions to define a common functional basis compared to levofloxacin.[27−29] We selected these MOFs (BTC-linked) because they are widely studied and synthetically mature, utilize readily available and industrially relevant precursors under the same chemistry, and span distinct metal chemistries and hotspot profiles, providing a controlled and representative basis for lab-to-industry LCA comparisons. Using OpenLCA with the Ecoinvent 3 database and the TRACI 2.1 impact assessment methodology, we quantified key impact categories, i.e., acidification, ecotoxicity, fossil fuel depletion, global warming potential, ozone depletion, and respiratory effects, as well as cumulative energy demand (CED). To integrate functional efficacy, we applied a dual-scenario framework: a functional scenario normalized to the mass required to fabricate 100,000 wound dressings (based on our minimum bactericidal concentration (MBC) assays where Ag-MOF achieved complete *Escherichia coli* (*E. coli*) inhibition at 0.1 mg L^{-1}, Cu-MOF at 25 mg L^{-1}, and Zn-MOF at 250 mg L^{-1}) and a nonfunctional scenario per 1000 kg of material produced. We then performed process-grouping analyses to identify the dominant environmental "hotspots" (e.g., silver precursor and ethanol) and projected large-scale production impacts to evaluate the benefits of industrial-scale synthesis.

2. MATERIALS AND METHODS

2.1. Synthesis of MOFs

Silver-based and copper-based MOFs were synthesized using benzene-1,3,5-tricarboxylic acid (BTC) as the organic linker, while a zinc-based MOF was prepared with benzimidazole as the ligand (Figure 1). In a typical procedure, 0.5 g of the metal nitrate ($AgNO_3$ for Ag-MOF, $Cu(NO_3)_2$ for Cu-MOF, and $Zn(NO_3)_2$ for Zn-MOF) was dissolved in 20 mL of deionized (DI) water under constant stirring to form the metal precursor solution. Separately, an equimolar amount of the corresponding ligand (BTC for Ag-MOF and Cu-MOF or benzimidazole for Zn-MOF) was dissolved in ethanol to prepare the ligand solution. The metal salt solution was then added to the ligand solution, and the mixture was subjected to pulsed ultrasonication (10 s on, 10 s off) for 1 h at ambient temperature. A solid MOF precipitate formed during sonication; this material was collected and washed with ethanol in three consecutive cycles to remove any unreacted ligand or metal precursor. The washed MOF products were finally dried in an oven (40 °C, overnight) and stored in a vacuum chamber for subsequent analysis.

2.2. Life Cycle Assessment Methodology (LCA)

A cradle-to-gate LCA was conducted for each antimicrobial agent (Ag-MOF, Cu-MOF, Zn-MOF, and levofloxacin) using OpenLCA software with the Ecoinvent 3 database as the background inventory source (Figure 2 and Figure S1). The life cycle inventory (LCI) for each material encompassed all relevant inputs (raw materials, chemicals, and energy) and outputs (emissions and wastes) associated with the synthesis of the active material. Environmental impact assessment was performed by characterizing the LCI data using the TRACI 2.1 methodology. Impact categories evaluated included acidification, ecotoxicity, fossil fuel depletion, global warming potential, ozone depletion, and respiratory effects (impact on human health via air pollutants). In addition to these impact categories, the CED was calculated and broken down by energy sources: nonrenewable fossil fuels, nonrenewable nuclear, and renewables (biomass, water or hydropower, and wind/solar/geothermal sources).

2.2.1. Functional Unit and System Boundary. The functional unit for the LCA was defined as the amount of antimicrobial material required to fabricate 100,000 wound dressings (each 14 mm × 5 mm in size) using 0.01 mL of MOF solution per dressing. This corresponds to normalizing all impacts to a per gram basis of the active agent, reflecting material consumption in a realistic application scenario. A mass-based functional unit was selected to accurately represent the usage of each antimicrobial in wound dressing fabrication and to provide a fair basis for

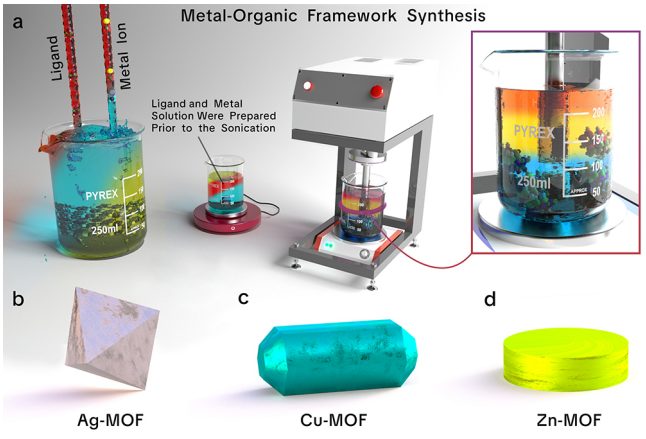

Figure 1. (a) Schematic representation of the synthesis route for Ag-MOF, Cu-MOF, and Zn-MOF. (b) Structural representation of Ag-MOF. (c) Schematic structure of Cu-MOF. (d) Schematic structure of Zn-MOF.

https://doi.org/10.1021/acssusresmgt.5c00499
ACS Sustain. Resour. Manag. 2026, 3, 717−732

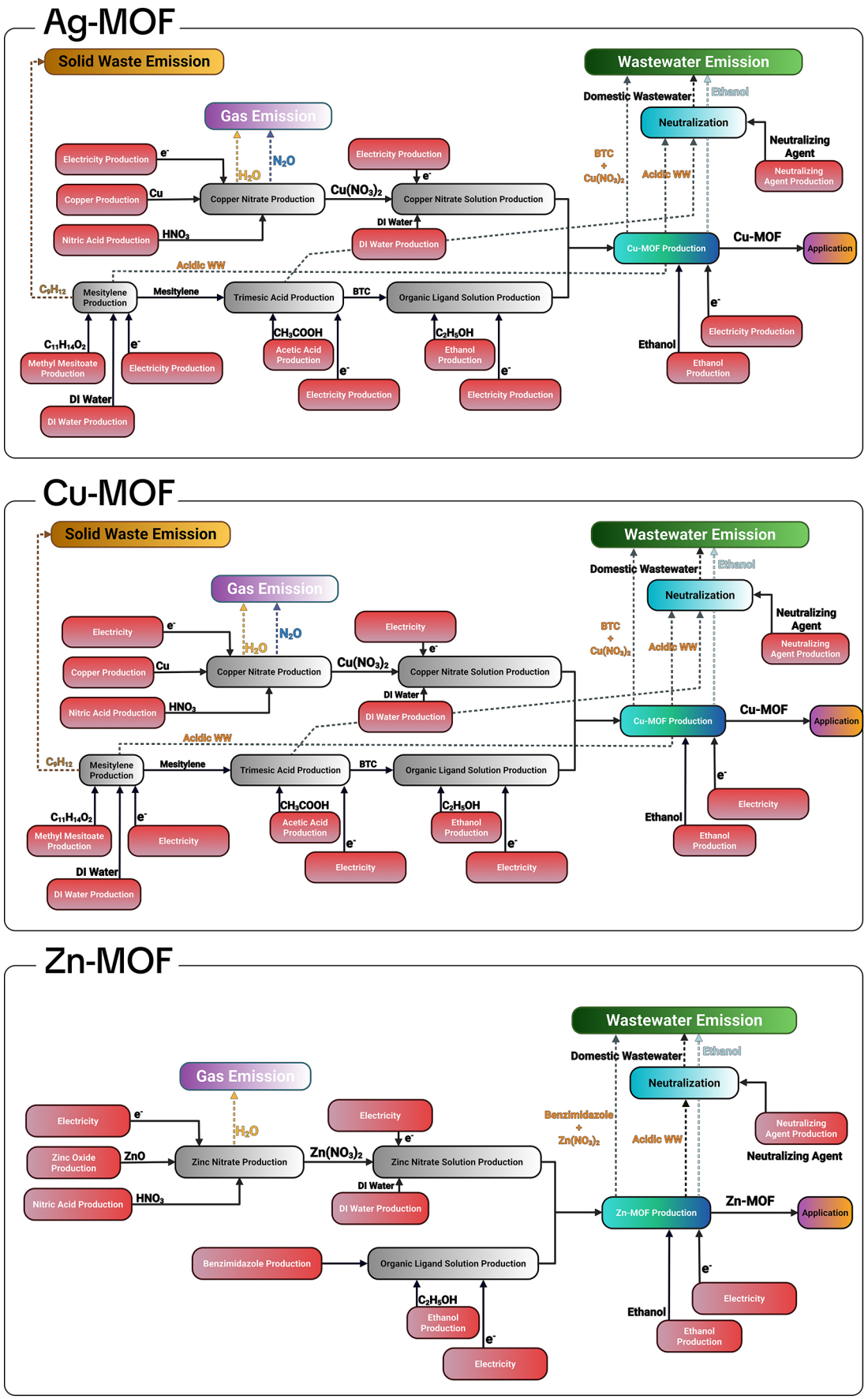

Figure 2. Overview of the LCA flow design for Ag-MOF, Cu-MOF, and Zn-MOF. The flowchart outlines the integration of life cycle inventory data to assess key environmental impact categories and cumulative energy demand within a cradle-to-gate framework.

https://doi.org/10.1021/acssusresmgt.5c00499
ACS Sustain. Resour. Manag. 2026, 3, 717−732

comparing the environmental burdens of the MOFs against the conventional antibiotic (levofloxacin). The system boundary was limited to cradle-to-gate processes, including raw material extraction and processing, precursor chemical production, energy consumption for synthesis (e.g., electricity for stirring, ultrasonication, and heating), and waste generation during MOF fabrication. Downstream processes, such as product distribution, use in wound dressings, and end-of-life disposal, were excluded from the LCA, as the focus was on the production-phase impacts of each material. Further methodological details and the complete life cycle inventory are provided in the Supporting Information (SI).

2.2.2. Lab-Scale versus Large-Scale Manufacturing Scenarios. In this work, two distinct fabrication scenarios were defined to assess the environmental impacts of MOF production under laboratory and industrial conditions. The lab-scale scenario strictly follows our day-to-day bench-scale protocols, which involve batch syntheses in small glassware volumes (typically ≤100 mL reactor size) and standard laboratory heating/stirring systems. All input and output flows (raw materials, energy, emissions, and wastes) reflect actual consumptions and losses observed during routine laboratory syntheses.

By contrast, the large-scale scenario retains the identical stoichiometry and reaction pathways but assumes translation to industrial-scale equipment and batch sizes (e.g., multiliter reactors with integrated heat exchangers, automated dosing, product filtration, and solvent recovery systems). Under this scenario, we model the same reagent ratios and reaction conditions but account for process intensification benefits such as improved energy efficiency through heat integration, reduced solvent losses via closed-loop recycling, and a lower per unit footprint due to economies of scale. All material and energy inputs are scaled proportionally to a 1000 kg annual production capacity, with equipment performance and recovery rates based on literature values for analogous industrial MOF syntheses.[30] This comparison isolates the sole effect of scale-up to reveal potential reductions in environmental burdens achievable through large-batch manufacturing under constant chemistries. All detailed life cycle inventory data for the highest contributing input streams are provided in the Supporting Information.

2.3. Antibacterial Testing

The antibacterial efficacy of the MOFs and levofloxacin was evaluated against *E. coli* F-AMP (ATCC strain 700891) using an MBC assay. Briefly, logarithmic-phase *E. coli* cultures were exposed to a series of two-fold dilutions of each test substance (Ag-MOF, Cu-MOF, Zn-MOF, or levofloxacin) in nutrient broth. The inoculated tubes were incubated at 37 °C for 3 h with orbital shaking at 100 rpm to allow the antimicrobial agents to interact with the bacteria. After a 3-h exposure period, 100 μL aliquots from each tube were plated onto Tryptic Soy Agar (TSA) plates, which were then incubated overnight at 37 °C. Bacterial growth was assessed the next day by counting colony-forming units (CFUs), and the MBC was defined as the lowest concentration of the MOF (or levofloxacin) that resulted in ≥99.9% reduction in *E. coli* colonies compared to the growth control. In practice, this corresponds to the lowest concentration at which no visible colonies grew on the agar plate after the overnight incubation, indicating effective bacterial inhibition. All MBC experiments were performed in triplicate to ensure reproducibility of the results.

2.4. Characterization of MOFs

The surface morphology and particle distribution of the synthesized MOFs were examined by scanning electron microscopy (SEM). Dried MOF samples were mounted on aluminum stubs and sputter-coated with a thin layer of gold to prevent charging. Imaging was performed at an accelerating voltage of 30 kV, and micrographs were recorded to observe the crystal habit and assess the uniformity of the MOF particles. Powder X-ray diffraction (XRD) was used to confirm the crystalline structure and phase purity of each MOF. XRD patterns were collected using a Cu K_α radiation source ($\lambda \approx 1.54$ Å) over a 2θ range of 5–50° at room temperature. The diffraction data for the Ag-MOF, Cu-MOF, and Zn-MOF samples were compared to reference patterns from the literature or database for the expected MOF structures. Matching peak positions and relative intensities confirmed the successful synthesis of the intended MOF phase in each case, with no significant impurity peaks observed.

3. RESULTS

3.1. MOFs Chemical Characterization

Figure 3 presents the chemical characterization of the synthesized MOFs via XRD and SEM characterizations. Figure 3a,

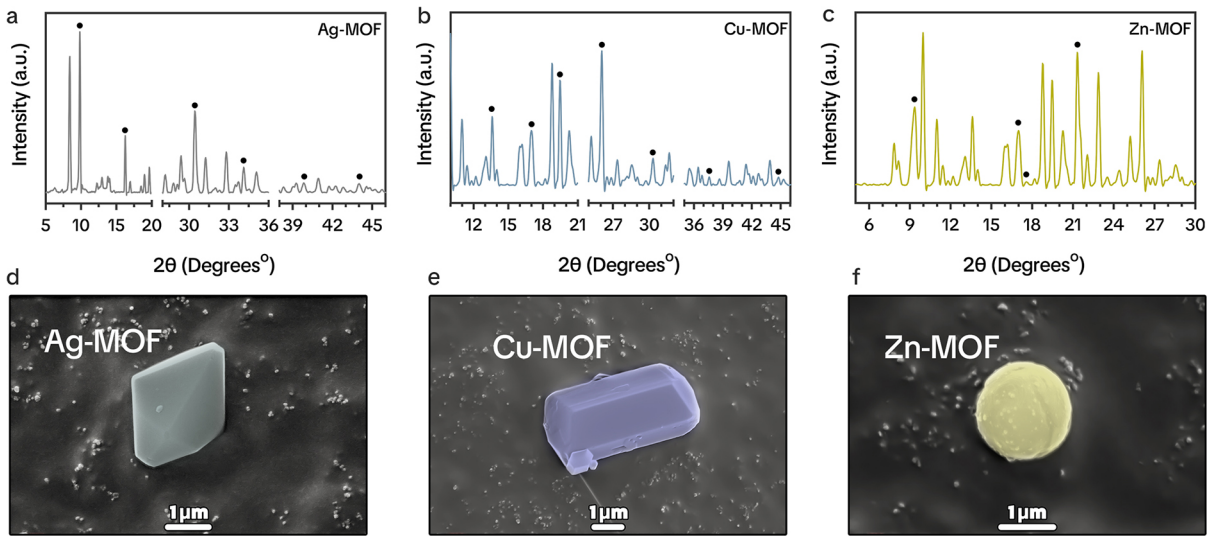

Figure 3. (a) XRD pattern of Ag-MOF showing characteristic peaks at 9.54, 16.2, and 30.4° along with additional peaks at 34.1, 40.1, and 44.4° corresponding to the (110), (111), and (200) planes of silver metal, respectively. (b) XRD pattern of Cu-MOF with peaks at 13.8, 19.6, and 30.0° and additional reflections at 13.8, 16.8, 26.0, 37.8, and 44.7° corresponding to the (101), (110), (103), (006), and (220) planes, respectively. (c) XRD pattern of Zn-MOF displaying peaks at 9.1, 16.7, 17.3, and 21.6° assigned to the (003), (125), (044), and (236) planes, respectively. (d–f) SEM images of Ag-MOF, Cu-MOF, and Zn-MOF, respectively, revealing a single, distinct crystalline structure for each material.

https://doi.org/10.1021/acssusresmgt.5c00499
ACS Sustain. Resour. Manag. 2026, 3, 717–732

Figure 3b, and Figure 3c display the XRD patterns of Ag-MOF, Cu-MOF, and Zn-MOF, respectively, while Figure 3d–f shows the corresponding SEM images.

The XRD pattern for Ag-MOF (Figure 3a) exhibits prominent peaks at 9.54, 16.2, and 30.4°, which align well with those documented in previous studies.[31,32] Notably, the sharp peak at 16.2° is indicative of a highly crystalline MOF structure. In addition, peaks at 34.1, 40.1, and 44.4° were observed and can be assigned to the (110), (111), and (200) planes of silver metal, respectively.[33,34] Analysis using Match software (version 4) against the Crystallography Open Database (COD) reference patterns provided further insight into potential additional phases (Table S2).

The XRD pattern for Cu-MOF (Figure 3b) shows peaks at 13.8, 19.6, and 30.0°, which are consistent with literature reports on Cu-MOFs.[35,36] Further detailed analysis revealed additional peaks at 13.8, 16.8, 26.0, 37.8, and 44.7°, corresponding to the (101), (110), (103), (006), and (220) planes, respectively.[37] Additional possible phases identified via Match software are presented in Table S3.

The XRD pattern for Zn-MOF (Figure 3c) displays peaks at 9.1, 16.7, 17.3, and 21.6°, which are in agreement with previously reported patterns for Zn-MOFs.[38] These peaks are assigned to the (003), (125), (044), and (236) planes, respectively.[39,40] Additional phases suggested by the Match software analysis are summarized in Table S4.

Complementary SEM images (Figure 3d–f) further confirm the presence of a single, distinct crystalline structure in each MOF. Each SEM micrograph clearly illustrates well-defined crystal facets consistent with the high crystallinity inferred from the XRD analyses. The combined XRD and SEM data validate the successful synthesis of Ag-MOF, Cu-MOF, and Zn-MOF, confirming that the crystal structures obtained are in close agreement with the literature and expected phase compositions.

3.2. MOFs Antibacterial Properties

Figure 4 illustrates the antibacterial evaluation of the MOFs. In Figure 4a, a schematic diagram shows the design of the wound dressing incorporating Ag-MOF, Cu-MOF, and Zn-MOF. Figure 4b displays representative agar plate photographs from the bacterial assay, including the control and samples treated with Ag-MOF, Cu-MOF, and Zn-MOF.

Quantitative analysis of the antibacterial performance is presented in Figure 4c–e. Figure 4c compares the inhibition profiles of Zn-MOF and levofloxacin. Zn-MOF exhibited a gradual increase in inhibition rate, reaching 45.8% at 10 mg L^{-1}, 71.6% at 25 mg L^{-1}, 82.6% at 75 mg L^{-1}, and ultimately achieving 100% inhibition at 250 mg L^{-1}. In contrast, levofloxacin demonstrated only moderate inhibition rates, with a maximum of 95.5% at a concentration of 500 mg L^{-1}.

Figure 4d details the antibacterial properties of Cu-MOF. Here, a rapid increase in efficacy is observed: Cu-MOF reached a 14.8% inhibition rate at 0.5 mg L^{-1}, 91.9% at 1 mg L^{-1}, 97.6% at 5 mg L^{-1}, and achieved complete (100%) inhibition at 25 mg L^{-1}, indicating its potent antibacterial action at relatively low concentrations.

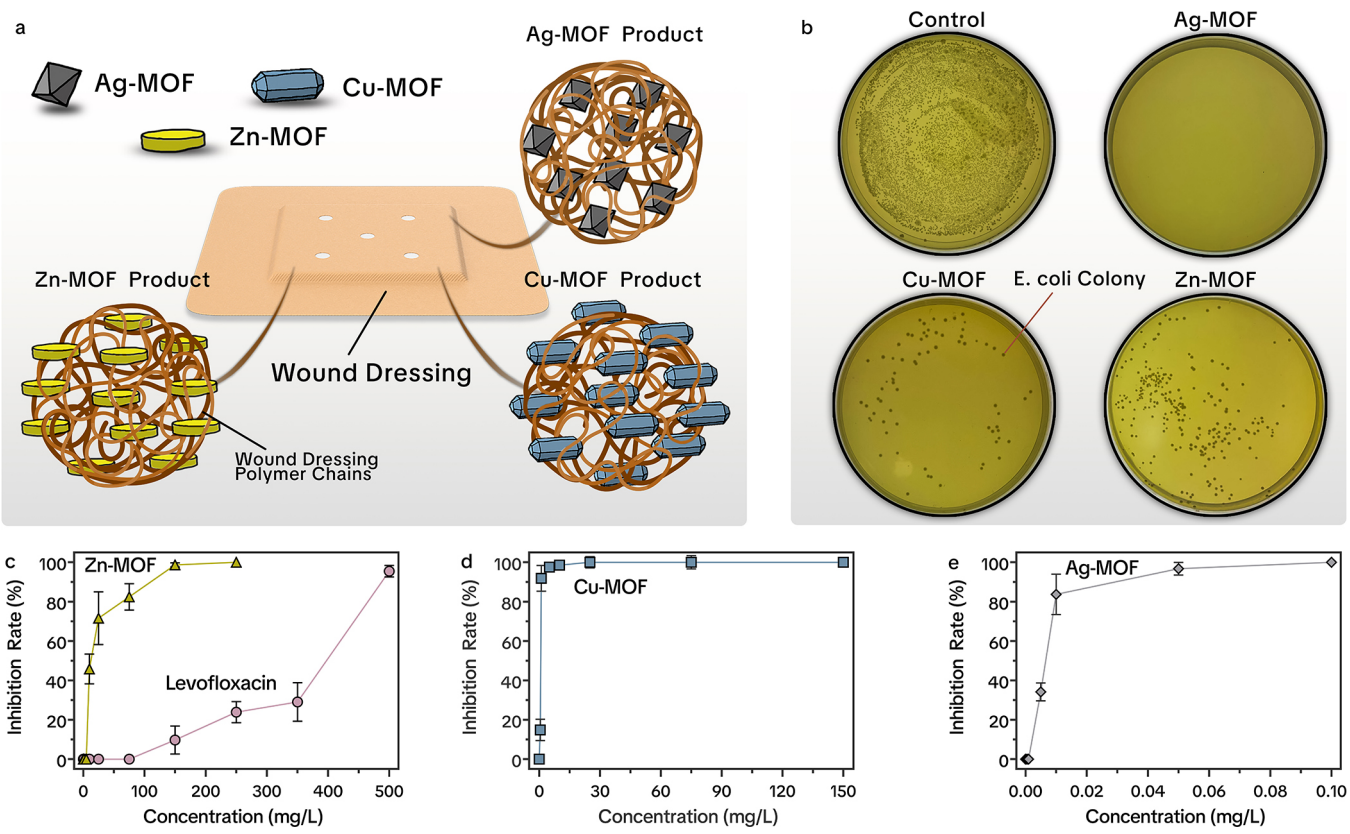

Figure 4. (a) Schematic illustration of the wound dressing design incorporating Ag-MOF, Cu-MOF, and Zn-MOF. (b) Representative agar plate photographs from the bacterial assay for the control sample and wound dressings loaded with Ag-MOF, Cu-MOF, and Zn-MOF. (c) Antibacterial activity profile of Zn-MOF compared with levofloxacin. (d) Concentration-dependent antibacterial efficacy of Cu-MOF. (e) Antibacterial performance of Ag-MOF, demonstrating potent inhibition at low dosages.

https://doi.org/10.1021/acssusresmgt.5c00499
ACS Sustain. Resour. Manag. 2026, 3, 717−732

Figure 4e presents the antibacterial performance of Ag-MOF, which exhibited the most remarkable activity among the tested agents. Ag-MOF showed no inhibition at very low concentrations (up to 0.001 mg L^{-1}), but its efficacy sharply increased to 34.2% at 0.005 mg L^{-1}, 83.74% at 0.01 mg L^{-1}, and reached complete inhibition (100%) at 0.1 mg L^{-1}. Collectively, these results indicate that while all MOFs possess antibacterial properties, Ag-MOF demonstrates superior efficacy at remarkably low dosages compared to Cu-MOF and Zn-MOF.

3.3. Life Cycle Assessment (LCA) of MOFs: Environmental Impacts Results

The environmental performance of Ag-MOF, Cu-MOF, Zn-MOF, and levofloxacin was evaluated using two complementary LCA approaches. In the functional scenario, impacts were normalized based on the quantity of the material required to fabricate 100,000 wound dressings (i.e., incorporating antibacterial efficacy). In the nonfunctional scenario, impacts were assessed per 1000 kg of material produced, independent of performance. The actual calculated impact data are presented in Table 1, while Figure 5 summarizes the normalized environmental impacts for the functional (Figure 5a) and nonfunctional (Figure 5b) scenarios.

Under the functional scenario, levofloxacin is set as the reference with a normalized impact of 100% in each impact category. Based on the actual calculated data (Table 1) and corresponding normalized values (Figure 5a), Ag-MOF exhibits markedly lower environmental impacts. For instance, in the acidification category, Ag-MOF registers a normalized impact of 0.04% (0.026 kg SO_2 eq, compared to 65.66 kg SO_2 eq for 50 kg of levofloxacin). Similarly, its impacts for fossil fuel depletion and global warming are as low as 0.02% relative to levofloxacin. Ecotoxicity for Ag-MOF is 1.08%, substantially lower than the 100% baseline.

In contrast, Cu-MOF displays normalized impacts of 0.57% for acidification, 7.75% for ecotoxicity, 0.18% for fossil fuel depletion, and 0.23% for global warming. Zn-MOF shows even higher normalized values in these categories, with acidification at 1.36%, ecotoxicity at 8.42%, fossil fuel depletion at 0.27%, and global warming at 0.35%. These higher normalized impacts reflect the greater mass of Cu-MOF and Zn-MOF required to achieve comparable antibacterial performance, as discussed in Section 3.2.

In the nonfunctional scenario, environmental impacts are reported per 1000 kg of production, and the normalized values are depicted in Figure 5b. Here, Ag-MOF exhibits a considerably higher environmental burden on a per-kilogram basis; for example, its acidification impact is calculated at 2611.21 kg SO_2 eq per 1000 kg, and the corresponding normalized value is set to 100%. In comparison, Cu-MOF and Zn-MOF show normalized acidification values of 14.4 and 22.74%, respectively. Similar trends are evident in ecotoxicity, fossil fuel depletion, and global warming categories. Although levofloxacin displays the highest impacts in some categories (e.g., fossil fuel depletion and ozone depletion at 100%), it records lower normalized values for acidification (50.29%) and global warming (93.24%) relative to Ag-MOF in this nonfunctional assessment.

While Ag-MOF exhibits high environmental burdens on a per kilogram basis (nonfunctional scenario), its exceptional antibacterial efficacy allows for a dramatically lower material input when normalized for functional performance. This results in normalized impacts as low as 0.02–1.08% across key categories. Conversely, Cu-MOF and Zn-MOF appear more sustainable from a bulk production perspective, yet their higher dosage requirements for effective antibacterial action lead to increased normalized impacts in the functional assessment.

3.4. Grouping of Environmental Impact Results

3.4.1. Effect of Input Flows. Figure 6 presents the normalized contributions of chemical, electricity, and waste inputs to the six environmental impact categories—acidification, ecotoxicity, fossil fuel depletion, global warming, ozone depletion, and respiratory effects—associated with the lab-scale synthesis of Ag-MOF, Cu-MOF, and Zn-MOF. The data reveal that chemical inputs are the dominant contributors across all impact categories. For acidification, chemicals account for 94.6% in Ag-MOF, 87.7% in Cu-MOF, and 89.5% in Zn-MOF, with electricity contributing between 5.1 and 11.7% and waste remaining below 1%. A similar trend is observed in the ecotoxicity category, where chemical contributions reach 97.4% for Ag-MOF, while Cu-MOF and Zn-MOF

Table 1. Environmental Impact Results for the Products Presented for Both the Functional (Impacts Are Normalized Based on the Mass Required to Fabricate 100,000 Wound Dressings) and the Nonfunctional Scenario (Impacts per 1000 kg of the Material Produced)

functional environmental impacts					
impact category	unit	levofloxacin	Ag-MOF (large scale)	Cu-MOF (large scale)	Zn-MOF (large scale)
acidification	kg SO_2 eq	65.66	0.026	0.38	0.89
ecotoxicity	CTUe	166909.63	1798.84	12943.78	14052.91
fossil fuel depletion	MJ surplus	17295.36	2.98	31.10	46.95
global warming	kg CO_2 eq	11913.25	2.56	27.56	41.20
ozone depletion	kg CFC-11 eq	0.017	2.63411E-07	3.93399E-06	5.87039E-06
respiratory effects	kg PM2.5 eq	8.83	0.004	0.03	0.078
nonfunctional environmental impacts					
impact category	unit	levofloxacin	Ag-MOF (large scale)	Cu-MOF (large scale)	Zn-MOF (large scale)
acidification	kg SO_2 eq	1313.11	2611.21	375.89	593.82
ecotoxicity	CTUe	3338192.66	179884073.01	12943782.25	9368603.78
fossil fuel depletion	MJ surplus	345907.15	298499.22	31100.93	31298.20
global warming	kg CO_2 eq	238264.97	255526.36	27562.57	27463.83
ozone depletion	kg CFC-11 eq	2.52E-01	2.63E-02	3.93E-03	3.91E-03
respiratory effects	kg PM2.5 eq	176.69	405.38	30.18	52.18

https://doi.org/10.1021/acssusresmgt.5c00499
ACS Sustain. Resour. Manag. 2026, 3, 717−732

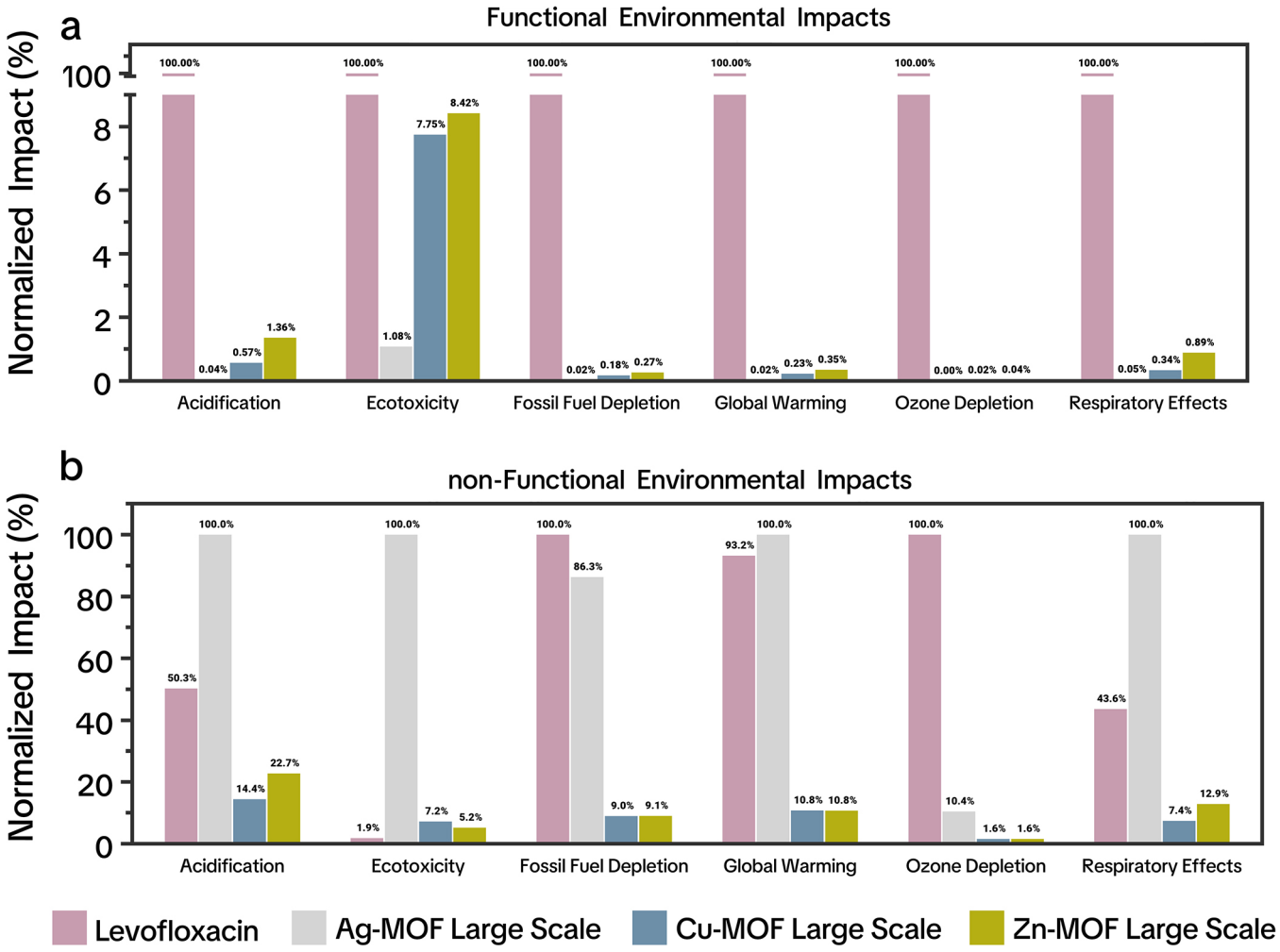

Figure 5. Normalized environmental impacts for the products evaluated under two scenarios: (a) functional scenario, where impacts are normalized based on the mass of the material required to fabricate 100,000 wound dressings, and (b) nonfunctional scenario, where impacts are assessed per 1000 kg of production. Impact categories include acidification, ecotoxicity, fossil fuel depletion, global warming, ozone depletion, and respiratory effects.

are characterized by lower chemical shares (78.1 and 74.2%, respectively) and correspondingly higher contributions from electricity (21.7 and 25.8%, respectively). In the fossil fuel depletion category, chemicals contribute 92.7% for Ag-MOF and approximately 80.8% for both Cu-MOF and Zn-MOF, with electricity accounting for 18.0% in Cu-MOF and 19.1% in Zn-MOF. Global warming impacts follow a comparable pattern, with chemical inputs responsible for 92.0% of Ag-MOF's impact and 81.7−82.6% for Cu-MOF and Zn-MOF, while electricity contributes 16.8−17.3%. Ozone depletion is similarly dominated by chemical flows (over 80% for all MOFs, reaching 91.4% in Ag-MOF), with electricity shares ranging from 8.4% in Ag-MOF to 17.0% in Zn-MOF; waste contributions remain minimal (<1%). Finally, for respiratory effects, chemicals are the primary contributors (92.5% for Ag-MOF, 79.4% for Cu-MOF, and 82.8% for Zn-MOF), with the electricity-related share increasing to 18.9% in Cu-MOF and 17.2% in Zn-MOF.

These results underscore that, in the lab-scale synthesis of these MOFs, chemical inputs are the primary drivers of environmental impacts. However, the contribution of electricity becomes more pronounced in the synthesis of Cu-MOF and Zn-MOF, particularly in terms of ecotoxicity, fossil fuel depletion, global warming, and respiratory effects. Waste flows are relatively minor across all categories.

3.4.2. Chemical Contribution Effect. *3.4.2.1. Ag-MOF Synthesis Input Contributions.* Figure 7 presents the relative contributions of individual chemicals—namely, silver, ethanol, nitric acid, naphtha, hydrogen, and water—to the six environmental impact categories associated with the lab-scale synthesis of Ag-MOF. In acidification, silver accounts for 62.74% of the impact, with ethanol contributing 36.88%. Ecotoxicity is overwhelmingly dominated by silver (96.27%), while ethanol has a smaller yet nontrivial share (3.72%). A similar trend is observed in fossil fuel depletion, where silver (66.89%) and ethanol (30.68%) together account for over 97% of the total burden, and in global warming, which is primarily driven by silver (61.85%) and ethanol (37.34%).

Notably, ozone depletion displays a more balanced distribution between silver (52.81%) and ethanol (44.84%), indicating that both the metal precursor and the organic solvent exert a comparable influence on this category. By contrast, respiratory effects mirror the trend observed in acidification, with silver accounting for 69.28% of the impact and ethanol contributing 30.53%. Other chemicals, including nitric acid, naphtha,

https://doi.org/10.1021/acssusresmgt.5c00499
ACS Sustain. Resour. Manag. 2026, 3, 717−732

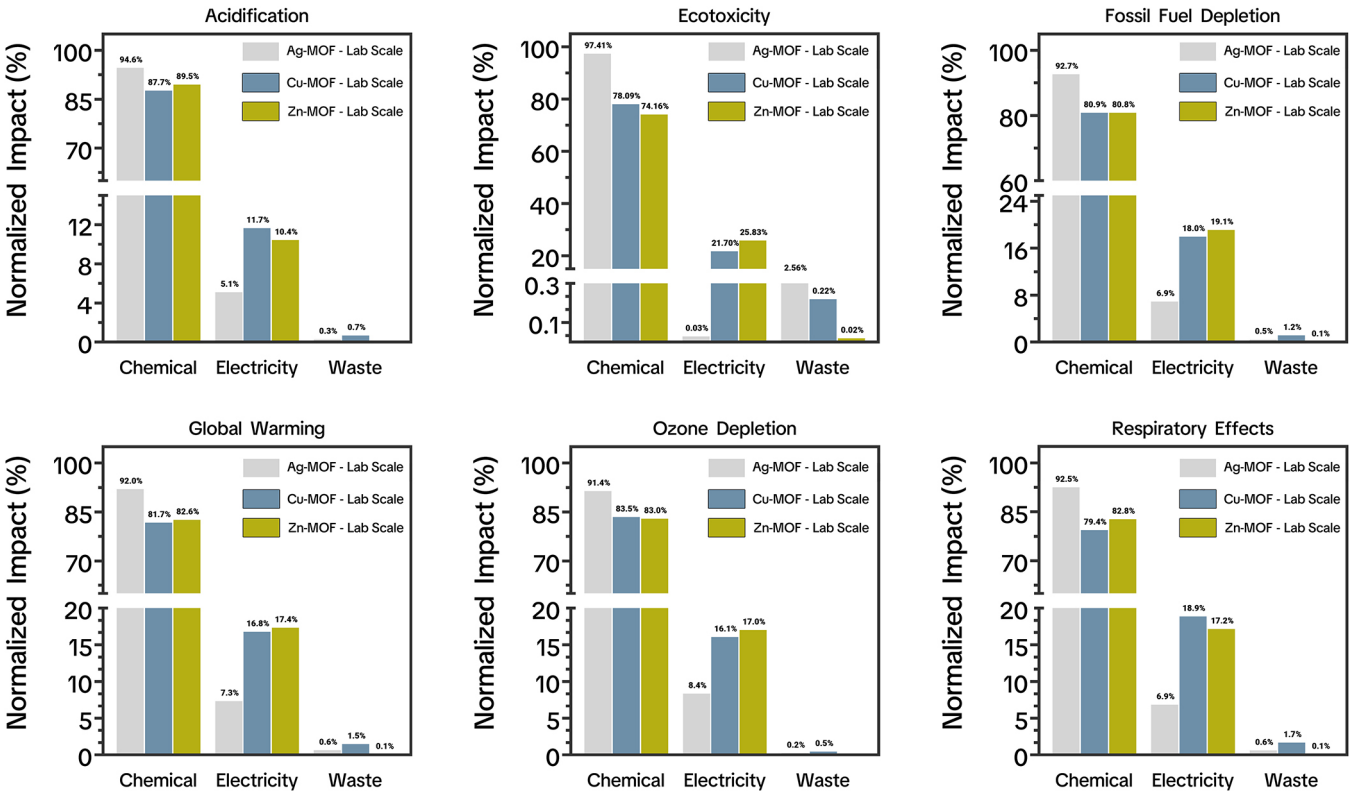

Figure 6. Normalized contributions of chemical, electricity, and waste inputs to the environmental impact categories for the lab-scale synthesis of Ag-MOF, Cu-MOF, and Zn-MOF. Impact categories include acidification, ecotoxicity, fossil fuel depletion, global warming, ozone depletion, and respiratory effects. Chemical inputs are the dominant contributors across all categories, while electricity exhibits notable contributions in the Cu-MOF and Zn-MOF synthesis, particularly in ecotoxicity, fossil fuel depletion, and global warming. Waste contributions remain minimal in all cases.

hydrogen, and water, exhibit negligible shares across all categories (<3% in most cases).

These findings highlight the significant contribution of silver to the environmental footprint of Ag-MOF synthesis, particularly in terms of ecotoxicity and respiratory effects. However, ethanol emerges as a substantial contributor to specific impact categories, such as ozone depletion. This chemical-level analysis highlights opportunities for targeted interventions, such as reducing or substituting the dominant chemicals, optimizing reaction protocols, and exploring more sustainable solvent systems, to mitigate the overall environmental impact of Ag-MOF production.

3.4.2.2. Cu-MOF Synthesis Input Contributions. Figure 8 illustrates the relative contributions of ethanol, copper, nitric acid, naphtha, hydrogen, and water to six environmental impact categories in the lab-scale synthesis of Cu-MOF. The data show that ethanol is the predominant contributor across most categories, particularly in acidification (98.08%) and ecotoxicity (94.19%). For fossil fuel depletion, ethanol accounts for the largest share (91.57%), with naphtha contributing 5.87%. Global warming impacts also reflect ethanol's influence at 80.50%, followed by nitric acid (11.85%) and copper (5.95%). In ozone depletion, ethanol still dominates (70.28%), but naphtha becomes more prominent (24.67%), whereas copper and hydrogen each contribute less than 3%. Respiratory effects are similarly driven by ethanol (90.91%), with copper (4.72%) and nitric acid (2.75%) having smaller, though non-negligible, shares.

These results highlight that the overall environmental footprint of Cu-MOF is strongly tied to the use of ethanol, which emerges as the principal impact driver across multiple categories. Although copper plays a noticeable role in some categories (e.g., ecotoxicity and global warming), its relative contribution is overshadowed by ethanol in most cases. Naphtha appears particularly relevant for ozone depletion, while nitric acid influences global warming to a moderate extent. By identifying ethanol as the primary source of environmental impacts, these findings underscore the importance of optimizing solvent use, exploring greener alternatives, or implementing more efficient process conditions to enhance the sustainability of Cu-MOF production.

3.4.2.3. Zn-MOF Synthesis Input Contributions. Figure 9 depicts the relative contributions of ethanol, benzimidazole, zinc sulfide, nitric acid, oxygen, and water to the six environmental impact categories for the lab-scale synthesis of Zn-MOF. In nearly all categories, ethanol dominates the overall impact. For example, it accounts for 83.93% of acidification, 95.4% of ecotoxicity, 91.5% of fossil fuel depletion, 95.19% of global warming, 95.21% of ozone depletion, and 89.34% of respiratory effects. Benzimidazole emerges as the second largest contributor, particularly in acidification (15.33%) and respiratory effects (10.15%), although its share remains below 5% in most other categories. Zinc sulfide and nitric acid each exhibit minor influences, generally less than 1% across all categories. Oxygen and water make negligible contributions (<0.1%) to every impact category.

These results underscore that ethanol consumption is the primary driver of environmental impacts in the lab-scale synthesis of Zn-MOF, similar to observations made for Cu-MOF. Benzimidazole also exhibits notable effects in acidification and respiratory impacts, suggesting that strategies to reduce or

https://doi.org/10.1021/acssusresmgt.5c00499
ACS Sustain. Resour. Manag. 2026, 3, 717−732

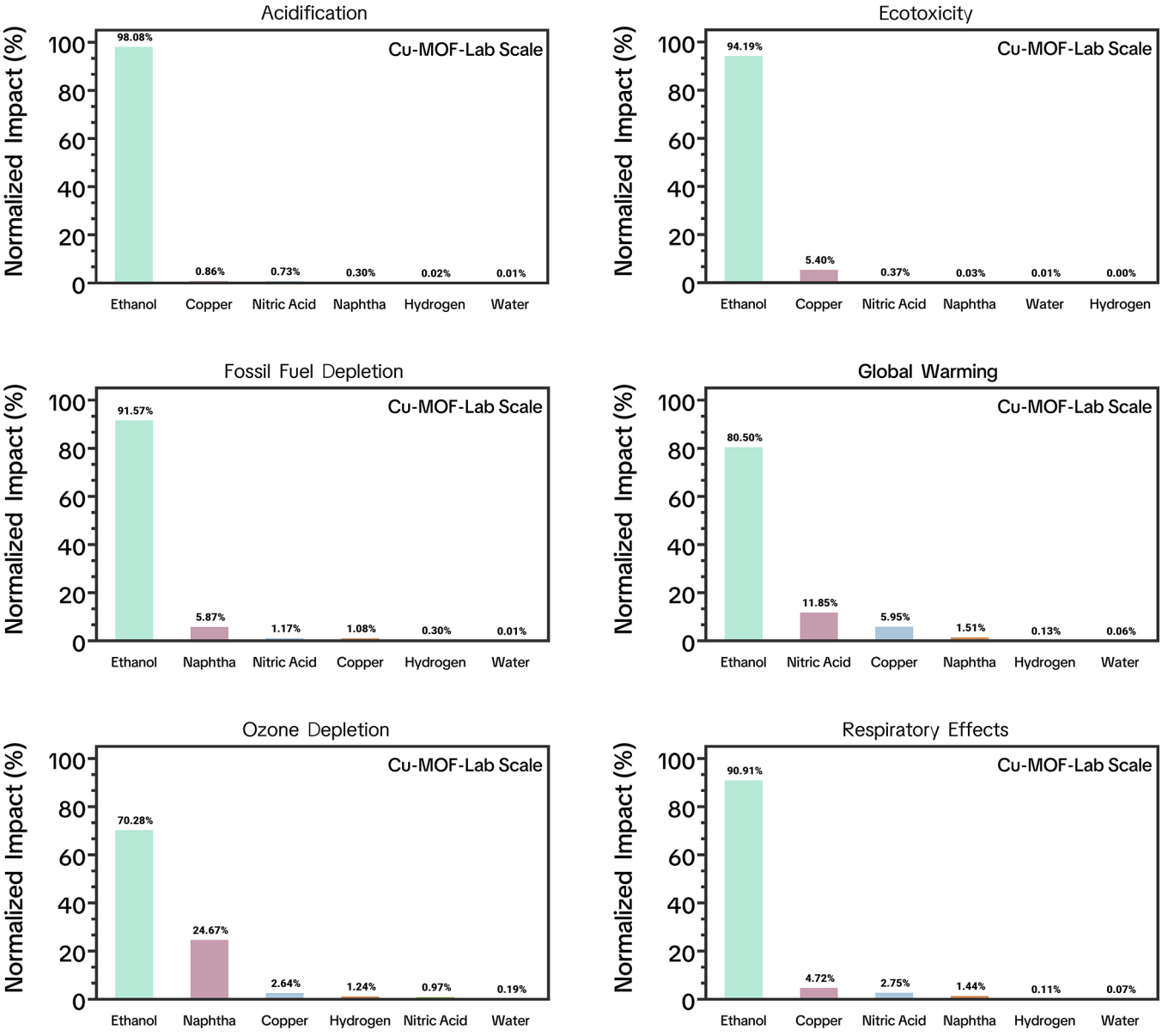

Figure 7. Relative contributions of silver, ethanol, nitric acid, naphtha, hydrogen, and water to six environmental impact categories in the lab-scale synthesis of Ag-MOF. Each panel illustrates the percentage share of these chemicals in acidification, ecotoxicity, fossil fuel depletion, global warming, ozone depletion, and respiratory effects, highlighting the dominant role of silver and ethanol in most categories.

substitute these two chemicals could substantially mitigate the overall environmental burden of Zn-MOF production.

The contribution analysis indicates that, unlike Ag-MOF, the metal precursors for Cu- and Zn-based MOFs do not emerge as dominant contributors, and this behavior can be directly explained by differences in metal abundance and refining pathways. Silver is a relatively scarce metal with a low crustal abundance and is typically obtained through energy-intensive mining and multistage refining processes, frequently as a byproduct of lead–zinc or copper ores. These characteristics lead to high upstream environmental burdens per kilogram of refined silver, which consequently dominate the life cycle impacts of Ag-MOF. In contrast, copper and zinc are significantly more abundant and are among the most widely produced industrial metals, with extraction and refining processes that have been extensively optimized over decades of large-scale production. The environmental impacts associated with Cu and Zn refining are therefore substantially lower on a per kilogram basis than those of silver and do not outweigh the impacts associated with solvent use in the MOF synthesis. As a result, ethanol, rather than the metal precursor, becomes the dominant contributor for Cu- and Zn-based MOFs in the contribution analysis. This comparison demonstrates that the lower impact of Cu and Zn metal precursors relative to silver is not a limitation of the assessment but a direct reflection of differences in metal abundance and refining intensity, which are explicitly captured in the life cycle inventory used in this study.

3.4.3. Effect of Manufacturing Optimization. Figure 10 compares the normalized environmental impacts for lab-scale and large-scale production of Ag-MOF (Figure 10a), Cu-MOF (Figure 10b), and Zn-MOF (Figure 10c) across six impact categories. In each panel, the lab-scale impacts are set to 100, allowing

https://doi.org/10.1021/acssusresmgt.5c00499
ACS Sustain. Resour. Manag. 2026, 3, 717−732

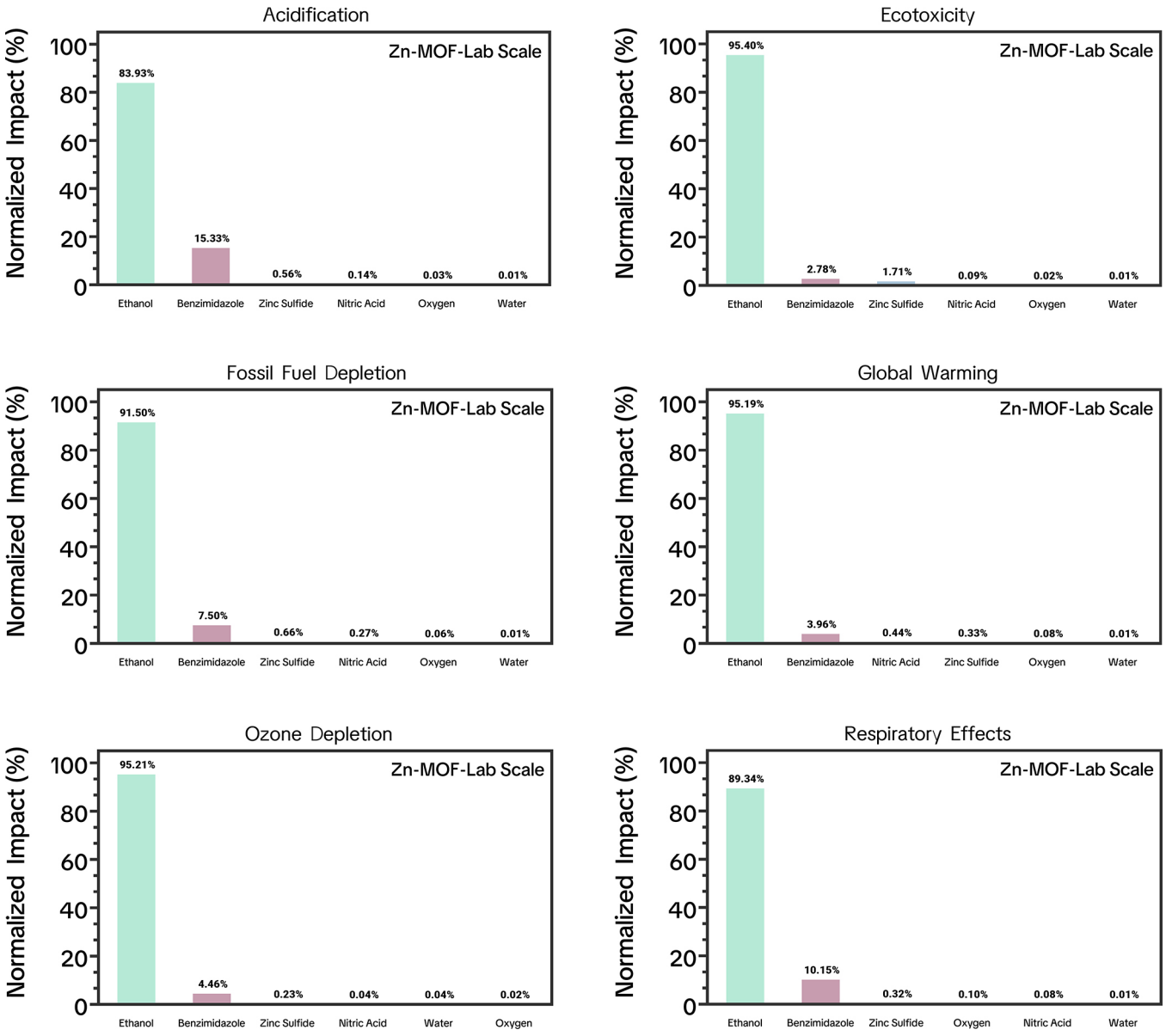

Figure 8. Relative contributions of ethanol, copper, nitric acid, naphtha, hydrogen, and water to six environmental impact categories (acidification, ecotoxicity, fossil fuel depletion, global warming, ozone depletion, and respiratory effects) in the lab-scale synthesis of Cu-MOF. The panels highlight ethanol as the principal driver in most categories, with copper, nitric acid, and naphtha exhibiting smaller but non-negligible impacts in select cases.

direct comparison with the large-scale values. For Ag-MOF (Figure 10a), large-scale production yields notable reductions in most categories, ranging from approximately 56.5% of the lab-scale impact for ozone depletion to 95.0% for ecotoxicity. Acidification, fossil fuel depletion, global warming, and respiratory effects each decrease to 64–69% of their lab-scale values. These reductions highlight the potential resource efficiencies and process optimizations achievable at industrial scales. However, the comparatively smaller decline in ecotoxicity suggests that certain inputs or byproducts may remain challenging to mitigate.

In the case of Cu-MOF (Figure 10b), the scale-up effect is even more pronounced. Large-scale acidification, fossil fuel depletion, and global warming impact each fall to 21, 18, and 15% of their respective lab-scale levels, while ozone depletion and respiratory effects similarly drop to 16 and 14%, respectively. Ecotoxicity decreases to 57%, indicating that although the overall footprint is substantially reduced, potential toxicological concerns persist. The dramatic improvements in most categories likely reflect greater energy efficiency and streamlined process design at larger production volumes. Zn-MOF (Figure 10c) also exhibits marked impact reductions upon scale-up. Large-scale acidification declines to 30% of the lab-scale impact, while fossil fuel depletion and global warming both drop to around 15–18%. Ecotoxicity decreases to 49%, ozone depletion to 16%, and respiratory effects to 22%. Although these values are not as low as those achieved by Cu-MOF under large-scale conditions, the data suggest that Zn-MOF manufacturing similarly benefits from economies of scale and improved resource utilization.

Overall, these findings highlight that transitioning from lab-scale to large-scale fabrication can yield substantial environmental benefits for MOFs, resulting to more efficient material utilization, reduced waste generation, and optimized energy consumption.

https://doi.org/10.1021/acssusresmgt.5c00499
ACS Sustain. Resour. Manag. 2026, 3, 717–732

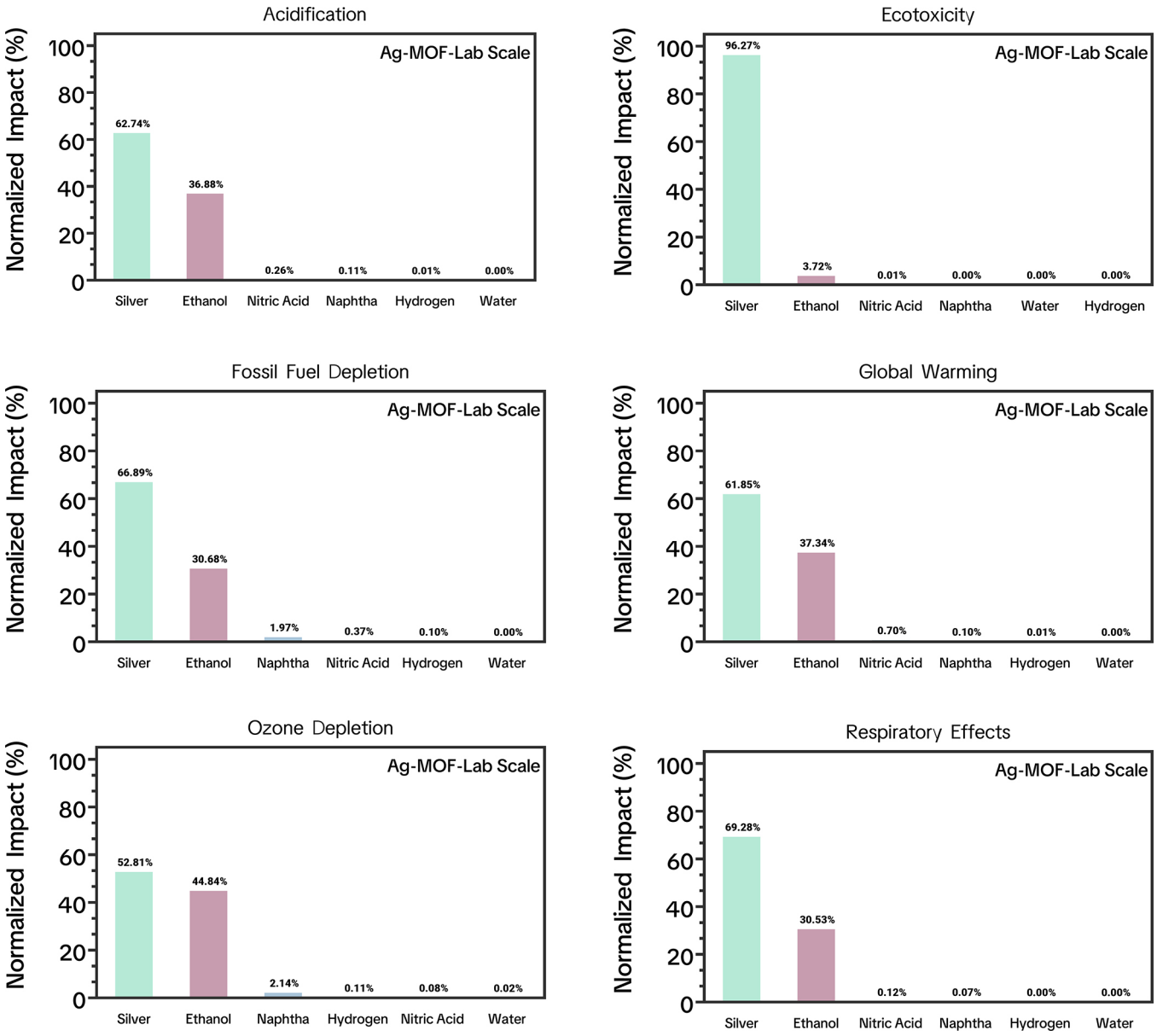

Figure 9. Relative contributions of ethanol, benzimidazole, zinc sulfide, nitric acid, oxygen, and water to six environmental impact categories (acidification, ecotoxicity, fossil fuel depletion, global warming, ozone depletion, and respiratory effects) in the lab-scale synthesis of Zn-MOF. Ethanol dominates the overall environmental burden across all categories, while benzimidazole shows a notable share in acidification and respiratory effects. Other chemicals contribute minimally in comparison.

However, certain impact categories, particularly ecotoxicity, remain comparatively higher in some MOFs even at larger scales, indicating the need for further process refinement and potential substitution of high-impact reagents to fully realize the sustainability potential of MOFs in industrial applications.

3.5. Cumulative Energy Demand (CED) of MOF Fabrication

Table 2 summarizes the actual CED values for levofloxacin, Ag-MOF (large scale), Cu-MOF (large scale), and Zn-MOF (large scale). These data encompass multiple energy sources, including fossil, nonrenewable biomass, nuclear, renewable biomass, water, and wind/solar/geothermal (WSG). To contextualize the impact of functionality (i.e., antibacterial efficacy), Figure 11 compares functional (Figure 11a) and nonfunctional (Figure 11b) normalized CED values, following the same approach used for the environmental impact assessment.

In the functional scenario (Figure 11a), levofloxacin is set to 100% for each energy source, providing a benchmark to which the MOFs are compared. Under this framework, all three MOFs exhibit markedly lower fossil energy demands, ranging from 0.02% (Ag-MOF) to 0.26% (Zn-MOF) relative to levofloxacin. A similar trend is observed for nuclear and water sources, where Cu-MOF and Zn-MOF remain below 1% in most categories, reflecting the considerably smaller mass of MOF required for equivalent antibacterial performance. However, renewable biomass usage increases more substantially for Cu-MOF (3.17%) and Zn-MOF (4.76%), suggesting that certain upstream processes for these materials, potentially related to raw material preparation, utilize renewable sources at a higher relative fraction.

https://doi.org/10.1021/acssusresmgt.5c00499
ACS Sustain. Resour. Manag. 2026, 3, 717−732

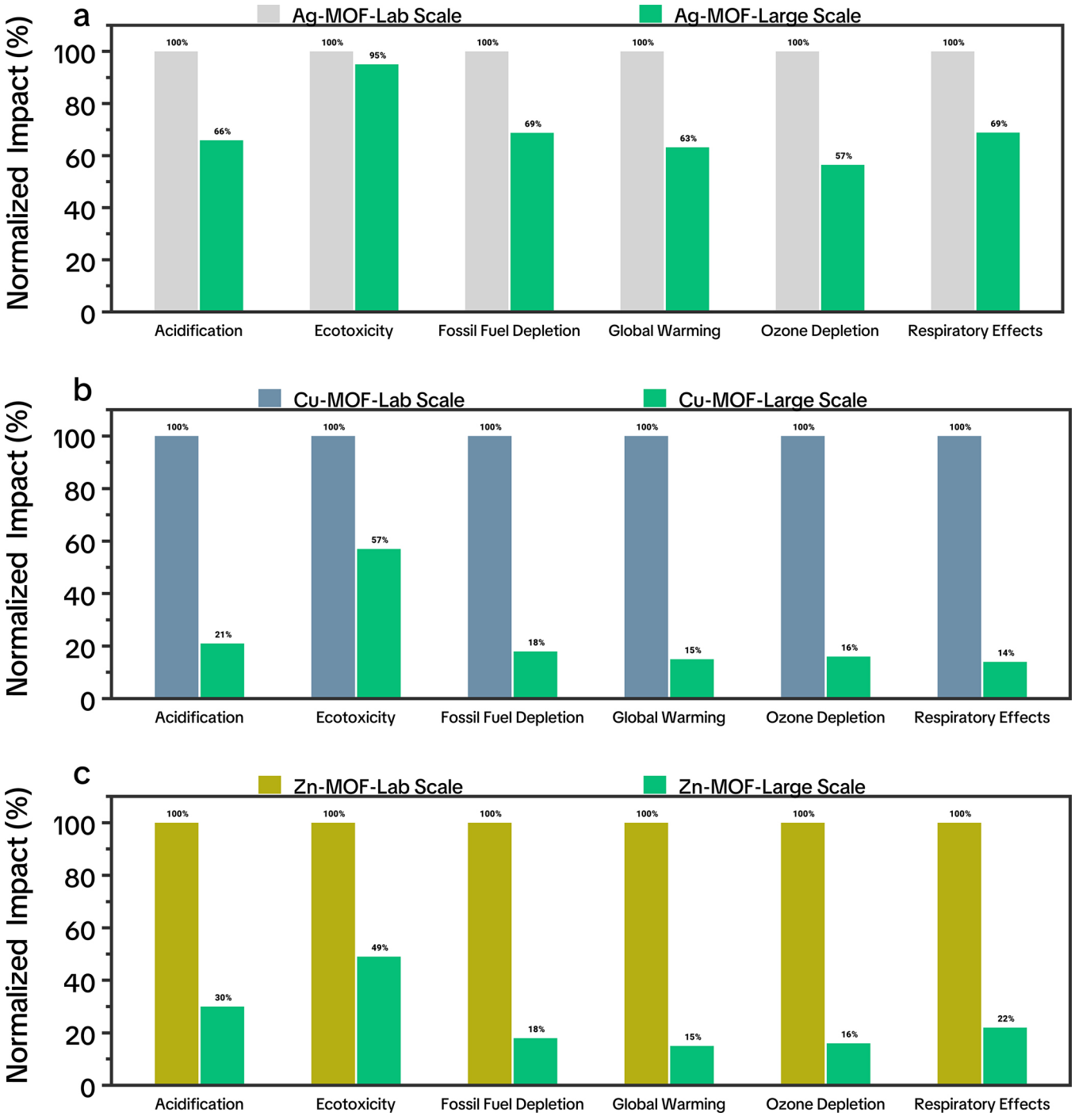

Figure 10. Normalized environmental impacts for lab-scale and large-scale production of (a) Ag-MOF, (b) Cu-MOF, and (c) Zn-MOF across six impact categories (acidification, ecotoxicity, fossil fuel depletion, global warming, ozone depletion, and respiratory effects). The data illustrate substantial reductions in most categories when transitioning from lab-scale to large-scale fabrication, highlighting the potential resource efficiencies and process optimizations achievable at larger production volumes.

In contrast, the nonfunctional scenario (Figure 11b) evaluates energy use per 1000 kg of material, regardless of antibacterial efficacy. Here, Ag-MOF is normalized to 100%, and levofloxacin appears comparable in some categories (e.g., fossil at 98.73%), while Cu-MOF and Zn-MOF exhibit notably lower demands (fossil at 8.46−8.58%). This reversal reflects the high resource intensity of scaling up Ag-MOF production. For instance, the nuclear energy usage for Cu-MOF (3.52%) and Zn-MOF (2.96%) remains substantially lower than that of Ag-MOF, implying that the bulk production of copper- or zinc-based frameworks may rely less heavily on nuclear-powered processes.

These findings align with the trade-offs identified in the environmental impact assessment. When viewed through a functional lens, Ag-MOF's strong antibacterial efficacy translates into lower overall energy demand, whereas nonfunctional analyses per kilogram show that large-scale silver-based production can be more

https://doi.org/10.1021/acssusresmgt.5c00499
ACS Sustain. Resour. Manag. 2026, 3, 717−732

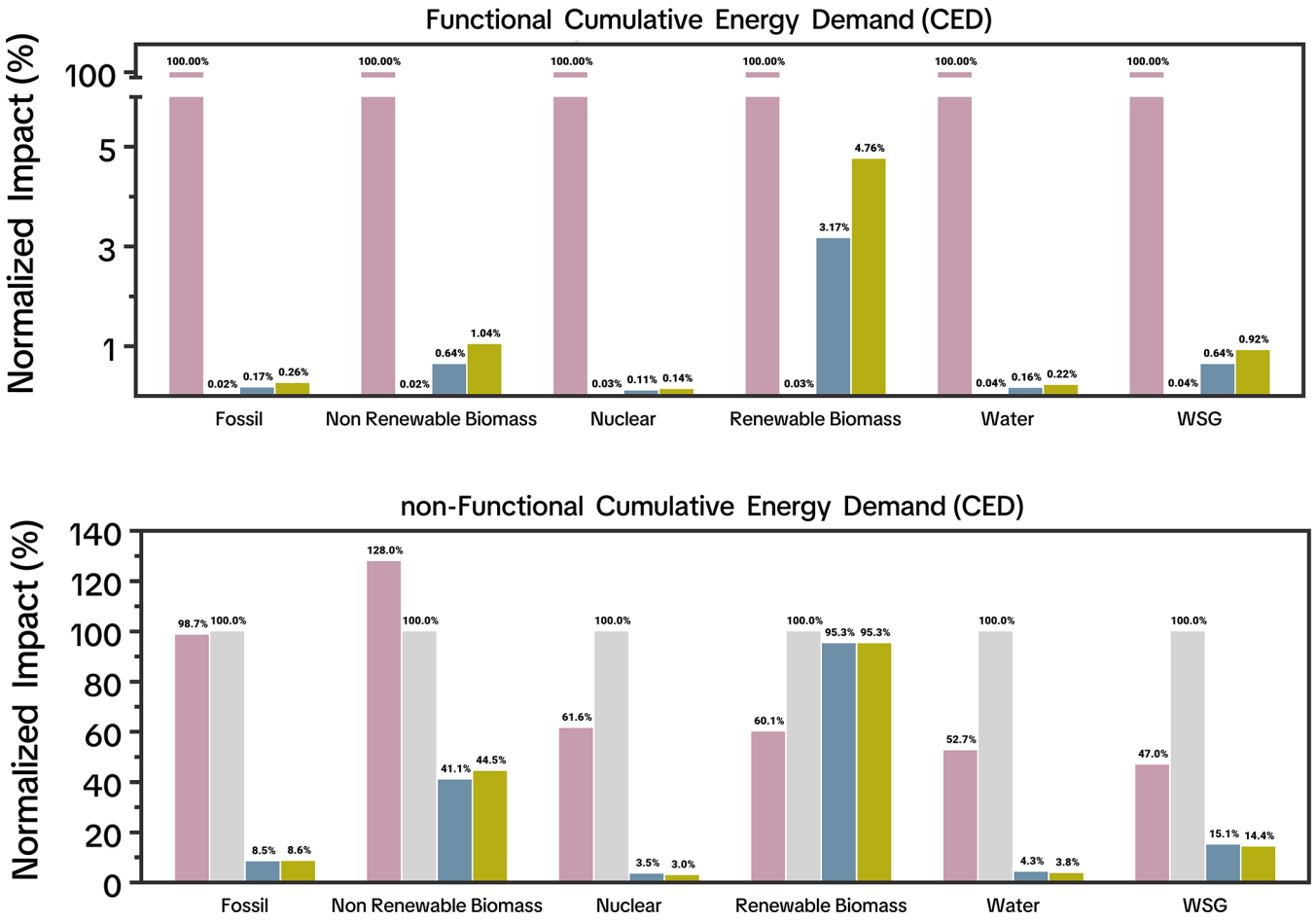

Figure 11. Normalized cumulative energy demand (CED) for the antibacterial agents evaluated under two scenarios: (A) functional scenario, where the CED is normalized based on the mass required to fabricate 100,000 wound dressings (benchmark: levofloxacin = 100%), and (B) nonfunctional scenario, where the CED is assessed per 1000 kg of production (benchmark: Ag-MOF = 100%). Energy sources include fossil fuels, nonrenewable biomass, nuclear energy, renewable biomass, water, and wind/solar/geothermal energy.

energy-intensive than Cu-MOF or Zn-MOF. These insights highlight the importance of considering both the inherent production burdens and the effective dose requirements when selecting the most sustainable antimicrobial materials.

4. DISCUSSION

Scaling up the MOF synthesis from bench-scale protocols to industrial production presents not only opportunities for greater efficiency but also challenges that conventional LCA frameworks may overlook. Our process-grouping analysis reveals that silver precursors and ethanol dominate the impacts of acidification, ecotoxicity, and ozone depletion under both laboratory- and large-scale scenarios, making them the first critical levers for sustainable scale-up. To mitigate silver-related burdens, future work should adopt closed-loop recovery, such as precipitating Ag^+ with 0.1 M Na_2S to form Ag_2S, followed by thermal reduction or electrowinning, to regenerate metallic silver. Simultaneously, solvent impacts can be minimized by replacing ethanol with greener alternatives, such as ethyl lactate (boiling point of 154 °C), which can reduce aquatic ecotoxicity by over 30%. This can be achieved by exploring bio-based alcohols or aqueous biphasic systems and integrating on-site distillation units capable of achieving ≥95% solvent recovery.

Batch sonication and heating steps, although adequate at the lab scale, become energy-intensive when scaled up. Researchers should explore continuous microreactor platforms for sonochemical or microwave-assisted MOF synthesis, offering superior mass/heat transfer and dramatically lower per unit energy demands. Alternatively, they can use modular heat integration strategies—such as coupling exothermic crystallization heat to preheat incoming feed, minimizing external thermal inputs, and flattening peak energy loads.

Another approach can focus on material innovation for circularity and multifunctionality. Beyond dosage normalization, achieving a true cradle-to-cradle paradigm will require designs that extend the utility of MOFs and enable end-of-life valorization. For example, instead of a single silver core metal, bimetallic or doped frameworks that reduce silver content while retaining antibacterial potency, e.g., Ag/Cu or Ag/Zn co-MOFs, can lower upstream burdens without sacrificing efficacy.

In contrasting the three MOF materials with the levofloxacin benchmark, several distinctive trade-offs become apparent. The Ag-MOF's exceptional potency, requiring only a fraction of the mass of levofloxacin to achieve equivalent bacterial inhibition, stems from its high silver content, yet this comes at the cost of substantial upstream impacts from the silver precursor synthesis and purification. In comparison, Cu-MOF and Zn-MOF

https://doi.org/10.1021/acssusresmgt.5c00499
ACS Sustain. Resour. Manag. 2026, 3, 717−732

Table 2. Cumulative Energy Demand (CED) for Levofloxacin, Ag-MOF (Large Scale), Cu-MOF (Large Scale), and Zn-MOF (Large Scale)[a]

functional cumulative energy demand (CED)					
impact category	unit	levofloxacin	Ag-MOF (large scale)	Cu-MOF (large scale)	Zn-MOF (large scale)
fossil	MJ-eq	155775.61	31.56	267.07	405.98
biomass[b]	MJ-eq	11.22	0.00	0.07	0.12
nuclear	MJ-eq	11520.73	3.74	13.19	16.60
biomass[c]	MJ-eq	30095.77	10.01	953.35	1431.24
water	MJ-eq	4319.14	1.64	7.02	9.45
WSG	MJ-eq	1321.09	0.56	8.50	12.11
total	MJ-eq	203043.57	47.51	1249.21	1875.49
			nonfunctional CED		
impact category	unit	levofloxacin	Ag-MOF (large scale)	Cu-MOF (large scale)	Zn-MOF (large scale)
fossil	MJ-eq	3115512.27	3155664.30	267070.81	270652.40
biomass[b]	MJ-eq	224.45	175.39	72.00	77.96
nuclear	MJ-eq	230414.70	374262.70	13190.27	11067.78
biomass[c]	MJ-eq	601915.39	1000897.85	953354.88	954160.54
water	MJ-eq	86382.73	163889.29	7018.52	6296.67
WSG	MJ-eq	26421.79	56235.70	8501.23	8074.26
total	MJ-eq	4060871.33	4751125.23	1249207.71	1250329.61

[a]The total CED (MJ-eq) is broken down by energy source—fossil, nonrenewable biomass, nuclear, renewable biomass, water, and wind/solar/geothermal (WSG)—illustrating the relative contributions of each to the overall energy footprint. [b]Nonrenewable. [c]Renewable.

demand higher dosages for the same antimicrobial effect but leverage more abundant, lower-impact metal salts and predominantly aqueous processing, resulting in a more balanced environmental profile when normalized to functional efficacy. Unlike levofloxacin, which relies on irreversible, multistep organic syntheses and faces mounting concerns over antimicrobial resistance and regulatory limits on antibiotic discharge, the crystalline MOF frameworks can be engineered for controlled ion release and even regenerated through mild chemical or thermal treatments, offering a route to circular material use that small-molecule drugs cannot match. The porous nature of MOFs affords tunable pore environments and co-ligation strategies for multipathogen targeting, in stark contrast to the single-mode mechanism of levofloxacin.

While wound-dressing fabrication provides a clear application case, broader deployment scenarios (e.g., water filtration cartridges and surface coatings in healthcare settings) should be evaluated. Defining functional units by service life, such as liters of water treated per gram of MOF or days of surface sterility, would guide the design of frameworks optimized simultaneously for performance longevity and minimal environmental footprint. To facilitate industrial adoption, future studies should couple LCA with techno-economic modeling. For example, developing cost-of-goods estimates that incorporate solvent recovery capital expenditures and metal recycling revenues or engage with regulatory stakeholders early to align process designs with environmental discharge limits for silver and solvent emissions ensures that scale-up strategies satisfy both economic and environmental compliance.

5. CONCLUSIONS

In this study, we evaluated the cradle-to-gate environmental performance of three prominent MOFs (Ag-MOF, Cu-MOF, and Zn-MOF) against the widely used antibiotic levofloxacin by normalizing all impacts to the dosage required for equivalent antibacterial efficacy. Our results reveal that, while Ag-MOF delivers the lowest functional mass per application, its silver-driven hotspots impose substantial upstream burdens; conversely, Cu-MOF and Zn-MOF offer more moderate impact profiles at the expense of higher material requirements. When scaled up to industrial levels, solvent recovery and metal-recycling strategies significantly reduce the environmental gap between MOFs and conventional antibiotic production, highlighting substantial opportunities for process intensification and circular design. By embedding experimentally measured minimum bactericidal concentrations (MBCs) into LCA metrics, this work establishes a rigorous framework for comparing emerging antimicrobial materials with commercial benchmarks and underscores the potential of MOF platforms to achieve sustainable, scalable alternatives to traditional pharmaceuticals.

■ ASSOCIATED CONTENT

Supporting Information

The Supporting Information is available free of charge at https://pubs.acs.org/doi/10.1021/acssusresmgt.5c00499.

Extended methodological details and additional results, including formal definitions of the TRACI 2.1 impact categories, full life cycle inventory (LCI) data, and flow diagrams for levofloxacin and the MOFs, supplementary characterization figures, expanded contribution and sensitivity analyses, and additional literature data on large-scale MOF synthesis and scale-up strategies that support the conclusions of this work (DOCX)

■ AUTHOR INFORMATION

Corresponding Authors

Mostafa Dadashi Firouzjaei – *Department of Civil, Construction, and Environmental Engineering, University of Alabama, Tuscaloosa, Alabama 35487, United States; Department of Mechanical Engineering, 10-241 Donadeo Innovation Center for Engineering, Advanced Water Research Lab (AWRL), University of Alberta, Edmonton, AB T6G*

https://doi.org/10.1021/acssusresmgt.5c00499
ACS Sustain. Resour. Manag. 2026, 3, 717−732

1H9, Canada; orcid.org/0000-0002-0215-8210; Email: mdfirouzjaei@ua.edu

Mark Elliott – *Department of Civil, Construction, and Environmental Engineering, University of Alabama, Tuscaloosa, Alabama 35487, United States;* orcid.org/0000-0002-7835-0612; Email: melliott@eng.ua.edu

Authors

Mohsen Pilevar – *Department of Civil, Construction, and Environmental Engineering, University of Alabama, Tuscaloosa, Alabama 35487, United States*

Rilyn Todd – *Department of Civil, Construction, and Environmental Engineering, University of Alabama, Tuscaloosa, Alabama 35487, United States; Chemical and Environmental Engineering, Yale University, New Haven, Connecticut 06520, United States*

Delanie Williams – *Department of Civil, Construction, and Environmental Engineering, University of Alabama, Tuscaloosa, Alabama 35487, United States*

Mahshid Mardani – *Department of Civil, Construction, and Environmental Engineering, University of Alabama, Tuscaloosa, Alabama 35487, United States*

Farhad Akbari Afkhami – *Department of Chemistry and Biochemistry, University of Alabama, Tuscaloosa, Alabama 35487, United States;* orcid.org/0000-0001-5977-8480

Mohtada Sadrzadeh – *Department of Mechanical Engineering, 10-241 Donadeo Innovation Center for Engineering, Advanced Water Research Lab (AWRL), University of Alberta, Edmonton, AB T6G 1H9, Canada;* orcid.org/0000-0002-0403-8351

Mona Bavarian – *Department of Chemical and Biomolecular Engineering, University of Nebraska-Lincoln, Lincoln, Nebraska 68588, United States;* orcid.org/0000-0001-7689-773X

Complete contact information is available at: https://pubs.acs.org/10.1021/acssusresmgt.5c00499

Author Contributions

[#]M.D.F. and M.P. contributed equally to this work.

Notes

The authors declare no competing financial interest.

■ ACKNOWLEDGMENTS

This research benefited greatly from funding provided by USDATAT-RWTS 00−69526, USEPA Cooperative Agreement MX-00D87019, The Richard Lounsbery Foundation, and the Transforming Wastewater Infrastructure in the United States project of Columbia World Projects. USDA or other agencies have not formally reviewed this paper, and the views expressed in this document are solely those of the authors and do not necessarily reflect those of the agencies.

■ REFERENCES

(1) Reddy, C. V.; Reddy, K. R.; Harish, V. V. N.; Shim, J.; Shankar, M. V.; Shetti, N. P.; Aminabhavi, T. M. Metal-organic frameworks (MOFs)-based efficient heterogeneous photocatalysts: Synthesis, properties and its applications in photocatalytic hydrogen generation, CO2 reduction and photodegradation of organic dyes. *Int. J. Hydrogen Energy* **2020**, *45* (13), 7656–7679.

(2) Dadashi Firouzjaei, M.; Shamsabadi, A. A.; Rahimpour, A.; Akbari Afkhami, F.; Elliott, M. Functionality review and life cycle assessment of a silver-based MOF for advanced material and sustainability applications. *Graphene 2D Mater.* **2024**, 227–244.

(3) Firouzjaei, M. D.; Shamsabadi, A. A.; Sharifian Gh, M.; Rahimpour, A.; Soroush, M. A novel nanocomposite with superior antibacterial activity: a silver-based metal organic framework embellished with graphene oxide. *Adv. Mater. Interfaces* **2018**, *5* (11), No. 1701365.

(4) Pilevar, M.; Jafarian, H.; Behzadnia, N.; Liang, Q.; Aghapour Aktij, S.; Thakur, A.; Gonzales, A. R.; Arabi Shamsabadi, A.; Anasori, B.; Warsinger, D. Analysis of Metal−Organic Framework and Polyamide Interfaces in Membranes for Water Treatment and Antibacterial Applications. *Small Methods* **2024**, *9* (4), No. 2401566.

(5) Seyedpour, S. F.; Arabi Shamsabadi, A.; Khoshhal Salestan, S.; Dadashi Firouzjaei, M.; Sharifian Gh, M.; Rahimpour, A.; Akbari Afkhami, F.; Shirzad Kebria, M. R.; Elliott, M. A.; Tiraferri, A. Tailoring the biocidal activity of novel silver-based metal azolate frameworks. *ACS Sustainable Chem. Eng.* **2020**, *8* (20), 7588–7599.

(6) Zolghadr, E.; Firouzjaei, M. D.; Aktij, S. A.; Aghaei, A.; Wujcik, E.; Sadrzadeh, M.; Rahimpour, A.; Afkhami, F.; LeClair, P.; Elliott, M. An ultrasonic-assisted rapid approach for sustainable fabrication of antibacterial and anti-biofouling membranes via metal-organic frameworks. *Mater. Today Chem.* **2022**, *26*, No. 101044.

(7) Bazrafshan, N.; Firouzjaei, M. D.; Elliott, M.; Moradkhani, A.; Rahimpour, A. Preparation and modification of low-fouling ultrafiltration membranes for cheese whey treatment by membrane bioreactor. *Case Stud. Chem. Environ. Eng.* **2021**, *4*, No. 100137.

(8) Firouzjaei, M. D.; Pejman, M.; Gh, M. S.; Aktij, S. A.; Zolghadr, E.; Rahimpour, A.; Sadrzadeh, M.; Shamsabadi, A. A.; Tiraferri, A.; Elliott, M. Functionalized polyamide membranes yield suppression of biofilm and planktonic bacteria while retaining flux and selectivity. *Sep. Purif. Technol.* **2022**, *282*, No. 119981.

(9) Pejman, M.; Firouzjaei, M. D.; Aktij, S. A.; Das, P.; Zolghadr, E.; Jafarian, H.; Shamsabadi, A. A.; Elliott, M.; Esfahani, M. R.; Sangermano, M. Improved antifouling and antibacterial properties of forward osmosis membranes through surface modification with zwitterions and silver-based metal organic frameworks. *J. Membr. Sci.* **2020**, *611*, No. 118352.

(10) Rezaeipour, Y.; Zolghadr, E.; Alizadeh, P.; Sadri, G.; Wujcik, E. K.; Afkhami, F. A.; Elliott, M.; Firouzjaei, M. D. The anticancer properties of metal-organic frameworks and their heterogeneous nanocomposites. *Biomater. Adv.* **2022**, *139*, No. 213013.

(11) He, Q.; Zhan, F.; Wang, H.; Xu, W.; Wang, H.; Chen, L. Recent progress of industrial preparation of metal−organic frameworks: synthesis strategies and outlook. *Mater. Today Sustain* **2022**, *17*, No. 100104.

(12) Al Obeidli, A.; Ben Salah, H.; Al Murisi, M.; Sabouni, R. Recent advancements in MOFs synthesis and their green applications. *Int. J. Hydrogen Energy* **2022**, *47* (4), 2561–2593.

(13) Kamal, K.; Bustam, M.; Ismail, M.; Grekov, D.; Shariff, A. M.; Pré, P. Optimization of Washing Processes in Solvothermal Synthesis of Nickel-Based MOF-74. *Materials* **2020**, *13*, 2741.

(14) Sandhu, Z. A.; Farwa, U.; Danish, M.; Raza, M. A.; Talib, A.; Amjad, H.; Riaz, R.; Al-Sehemi, A. G. Sustainability and photocatalytic performance of MOFs: Synthesis strategies and structural insights. *J. Cleaner Prod* **2024**, *470*, No. 143263.

(15) Zhao, T.; Peng, S.; Yu, J.; Chen, J.; Luo, F.; Xiao, P.; Nie, S.; Chen, Y. Advances in Green Synthesis and Photo-/Electrocatalytic Applications of Zirconium-Based MOFs: A Review. *Organics* **2025**, *6* (2), 22.

(16) Escobar-Hernandez, H.; Quan, Y.; Papadaki, M.; Wang, Q. Life Cycle Assessment of Metal−Organic Frameworks: Sustainability Study of Zeolitic Imidazolate Framework-67. *ACS Sustainable Chem. Eng.* **2023**, *11* (10), 4219–4225.

(17) Hu, Z.; Wang, Y.; Zhao, D. Modulated Hydrothermal Chemistry of Metal−Organic Frameworks. *Acc. Mater. Res.* **2022**, *3* (11), 1106–1114.

(18) Aghapour Aktij, S.; Dadashi Firouzjaei, M.; Pilevar, M.; Asad, A.; Rahimpour, A.; Elliott, M.; Soares, J. B. P.; Sadrzadeh, M. Enhancing sustainable energy production through co-polyamide membranes for

improved pressure-retarded osmosis performance and environmental impact: synthesis and life cycle analysis. *Green Chem.* **2025**, *27* (3), 586–606.
(19) Moradi, K.; Firouzjaei, M. D.; Elliott, M.; Sadrzadeh, M. Lifecycle assessment of membrane synthesis for the application of thermo-osmotic energy conversion process. *Case Stud. Chem. Environ. Eng.* **2024**, *10*, No. 100847.
(20) Dadashi Firouzjaei, M.; Nemani, S. K.; Sadrzadeh, M.; Wujcik, E. K.; Elliott, M.; Anasori, B. Life-Cycle Assessment of Ti3C2Tx MXene Synthesis. *Adv. Mater.* **2023**, *35* (31), No. 2300422.
(21) Yang, H.; Zhao, Y.; Guo, Y.; Wu, B.; Ying, Y.; Sofer, Z.; Wang, S. Surfactant-Mediated Crystalline Structure Evolution Enabling the Ultrafast Green Synthesis of Bismuth-MOF in Aqueous Condition. *Small* **2023**, *20* (15).
(22) Assen, A.; Adil, K.; Belmabkhout, Y. Lab-scale insights into green metal-organic framework sorbents for gas separation or purification. *Curr. Opin. Green Sustainable Chem.* **2024**, *19*, No. 100948.
(23) Sun, Y.; Bai, S.; Wang, X.; Ren, N.; You, S. Prospective Life Cycle Assessment for the Electrochemical Oxidation Wastewater Treatment Process: From Laboratory to Industrial Scale. *Environ. Sci. Technol.* **2023**, *57* (3), 1456.
(24) Xia, W.; Lau, S. K.; Yong, W. F. Comparative life cycle assessment on zeolitic imidazolate framework-8 (ZIF-8) production for CO2 capture. *J. Cleaner Prod.* **2022**, *370*, No. 133354.
(25) Dutta, S.; Walden, M.; Sinelshchikova, A.; Ettlinger, R.; Lizundia, E.; Wuttke, S. Cradle-to-Gate Environmental Impact Assessment of Commercially Available Metal-Organic Frameworks Manufacturing. *Adv. Funct. Mater.* **2024**, *34*, No. 2410751.
(26) Abazari, R.; Sanati, S.; Bajaber, M.; Javed, M. S.; Junk, P.; Nanjundan, A.; Qian, J.; Dubal, D. Design and Advanced Manufacturing of NU-1000 Metal-Organic Frameworks with Future Perspectives for Environmental and Renewable Energy Applications. *Small* **2023**, *20*, No. 2306353.
(27) Liu, M.; Guinart, A.; Granados, A.; Gimbert-Suriñach, C.; Fernández, E.; Pleixats, R.; Vallribera, A. Coated Cotton Fabrics with Antibacterial and Anti-Inflammatory Silica Nanoparticles for Improving Wound Healing. *ACS Appl. Mater. Interfaces.* **2024**, *16*, 14595–14604.
(28) Suhail, Z.; Shoukat, H.; Sanbhal, N.; Chowdhry, N.; Bhutto, M.; Soomro, S.; Ansari, A.; Memon, R. Controlled Drug Release and Antibacterial Properties of Levofloxacin-Loaded Silk/Chitosan Green Composite for Wound Dressing. *Biomed. Mater. Devices* **2022**, *1*, 796–804.
(29) Peng, K.; Li, M.; Himawan, A.; Domínguez-Robles, J.; Vora, L.; Duncan, R.; Dai, X.; Zhang, C.; Zhao, L.; Li, L.; et al. Amphotericin B- and Levofloxacin-Loaded Chitosan Films for Potential Use in Antimicrobial Wound Dressings: Analytical Method Development and Its Application. *Pharmaceutics* **2022**, *14*, 2497.
(30) Wang, G.-D.; Li, Y.-Z.; Krishna, R.; Zhang, W.; Hou, L.; Wang, Y.-Y.; Zhu, Z. Scalable Synthesis of Robust MOF for Challenging Ethylene Purification and Propylene Recovery with Record Productivity. *Angew. Chem.* **2024**, *136*, No. e202319978.
(31) Kwon, D.; Kim, J. Ag metal organic frameworks nanocomposite modified electrode for simultaneous electrochemical detection of copper (II) and lead (II). *J. Appl. Electrochem.* **2021**, *51* (8), 1207–1216.
(32) Hu, Y.; Yang, H.; Wang, R.; Duan, M. Fabricating Ag@ MOF-5 nanoplates by the template of MOF-5 and evaluating its antibacterial activity. *Colloids Surf. A Physicochem. Eng. Asp.* **2021**, *626*, No. 127093.
(33) Chen, Q.; Zhou, M.; Fu, Y.; Weng, J.; Zhang, Y.; Yue, L.; Xie, F.; Huo, C. Magnetron sputtering synthesis silver and organic PEO nanocomposite. *Surf. Coat. Technol.* **2008**, *202* (22-23), 5576–5578.
(34) Kang, S.; Nikles, D.; Harrell, J. Synthesis, chemical ordering, and magnetic properties of self-assembled FePt−Ag nanoparticles. *J. Appl. Phys.* **2003**, *93* (10), 7178–7180.
(35) Abdelmoaty, A. S.; El-Beih, A. A.; Hanna, A. A. Synthesis, characterization and antimicrobial activity of copper-metal organic framework (Cu-MOF) and its modification by melamine. *J. Inorg. Organomet. Polym. Mater.* **2022**, *32* (5), 1778–1785.
(36) Zang, L.; Qiu, J.; Yang, C.; Sakai, E. Preparation and application of conducting polymer/Ag/clay composite nanoparticles formed by in situ UV-induced dispersion polymerization. *Sci. Rep.* **2016**, *6* (1), No. 20470.
(37) Khan, J.; Iqbal, M. Z.; Rubab, B.; Jamshaid, F.; Khan, A.; Shakeel, N.; Ahmed, A.; Al-Kahtani, A. A. Isonicotinic acid-based copper-MOF: An exotic redox propertied electrode material for high energy asymmetric supercapacitor. *J. Energy Storage* **2023**, *72*, No. 108655.
(38) Alibakhshi, S.; Shahvelayati, A. S.; Sheshmani, S.; Ranjbar, M.; Souzangarzadeh, S. Design, synthesis, and characterization of a novel Zn (II)-2-phenyl benzimidazole framework for the removal of organic dyes. *Sci. Rep.* **2022**, *12* (1), 12431.
(39) Park, K. S.; Ni, Z.; Côté, A. P.; Choi, J. Y.; Huang, R.; Uribe-Romo, F. J.; Chae, H. K.; O'Keeffe, M.; Yaghi, O. M. Exceptional chemical and thermal stability of zeolitic imidazolate frameworks. *Proc. Natl. Acad. Sci.* **2006**, *103* (27), 10186–10191.
(40) Yao, J.; He, M.; Wang, K.; Chen, R.; Zhong, Z.; Wang, H. High-yield synthesis of zeolitic imidazolate frameworks from stoichiometric metal and ligand precursor aqueous solutions at room temperature. *CrystEngComm* **2013**, *15* (18), 3601–3606.

https://doi.org/10.1021/acssusresmgt.5c00499
ACS Sustain. Resour. Manag. 2026, 3, 717–732